

# Mathematical Billiards

Lucy Dhumeaux

November 2023

## Contents

<b>1</b>	<b>Background maths</b>	<b>2</b>
1.1	Chaos Theory . . . . .	2
1.2	2D billiards . . . . .	3
<b>2</b>	<b>Integrable billiards</b>	<b>5</b>
2.1	The square . . . . .	5
2.2	The circle . . . . .	6
2.3	The ellipse . . . . .	10
<b>3</b>	<b>Chaotic billiards</b>	<b>13</b>
3.1	The Bunimovich stadium . . . . .	13
3.2	The half stadium . . . . .	18

## Introduction

Mathematical billiards are an idealization of the billiard game, in which a point mass moves in straight line and collides elastically with a boundary [1]. The dynamics of a billiard are governed by Hamilton's equations, but these don't need to be integrated to solve the system. This is because the dynamics are simple enough that the future state of the system can be determined directly from the current state. Also, the dynamics are discrete: they are characterized by the points of collision with the boundary. Billiards are usually described by a map  $B$  that gives the next point  $\mathbf{x}_{n+1}$  from the current point  $\mathbf{x}_n$ :

$$B(\mathbf{x}_n) = \mathbf{x}_{n+1}$$

Despite being elementary, dynamical billiards have complex behaviour. Some systems are integrable, and some are chaotic. Integrable billiards make good models for many concepts physics, like thermodynamics [2], optics, laser, quantum mechanics... Chaotic billiards, as we will see, are straightforward to simulate and give a simple insight into chaos theory.

We investigate the square, the circle, the ellipse, the Bunimovich stadium and the half stadium. The first three systems are integrable. The square and the circle have a lot of symmetries, so they have extra conserved quantities and are easy to solve. The ellipse happens to have a 'geometric integrability' that makes it completely predictable [3].

The Bunimovich stadium [4] and the half stadium, on the other hand, are chaotic. The combination of straight and curved segments creates a wide range of possible angles the ball can take. This leads to complex trajectories, and sensitivity to initial conditions.

We start by recalling some notions from chaos theory, then explain our approach to solving dynamical billiards. We compare our results for integrable billiards with analytic solutions, then characterise chaos in the stadiums with the Lyapunov exponent.

## 1 Background maths

### 1.1 Chaos Theory

Systems with at least as many conserved quantities as degrees of freedom are said to be integrable. They have regular motion, and are predictable. Examples of such systems are the square, circle and ellipse billiard.

Chaotic systems are sensitive to initial conditions and have complex motion that makes them unpredictable, although they are deterministic. There are no 'right' conditions that a system can fulfil to be classified as chaotic, so we chose to take sensitivity to initial condition as our requirement for chaos.

This sensitivity is characterised using the Lyapunov exponent. The Lyapunov quantifies the exponential growth of the difference in trajectory between two infinitesimally close initial conditions.

Consider the billiard map on an initial point in phase space  $B(\mathbf{x}_1)$  and on the infinitesimally close point  $B(\mathbf{x}_1 + \delta\mathbf{x}) = B(\mathbf{x}_1) + \delta\mathbf{x}B'(\mathbf{x}_1)$ , where we take the first order Taylor expansion. Applying the map again, we have  $B^2(\mathbf{x}_1)$  and

$$\begin{aligned} B^2(\mathbf{x}_1 + \delta\mathbf{x}) &= B(B(\mathbf{x}_1) + \delta\mathbf{x}B'(\mathbf{x}_1)) \\ &= B^2(\mathbf{x}_1) + \delta\mathbf{x}B'(\mathbf{x}_1)B'(B(\mathbf{x}_1)) \\ &= B^2(\mathbf{x}_1) + \delta\mathbf{x}B'(\mathbf{x}_1)B'(\mathbf{x}_2) \end{aligned}$$

The third points are  $B^3(\mathbf{x}_1)$  and

$$\begin{aligned} B^3(\mathbf{x}_1 + \delta\mathbf{x}) &= B(B^2(\mathbf{x}_1) + \delta\mathbf{x}B'(\mathbf{x}_1)B'(\mathbf{x}_2)) \\ &= B^3(\mathbf{x}_1) + \delta\mathbf{x}B'(\mathbf{x}_1)B'(\mathbf{x}_2)B'(B^2(\mathbf{x}_1)) \\ &= B^3(\mathbf{x}_1) + \delta\mathbf{x}B'(\mathbf{x}_1)B'(\mathbf{x}_2)B'(\mathbf{x}_3) \end{aligned}$$

Then  $N$  applications of the map gives

$$|B^N(\mathbf{x}_1) - B^N(\mathbf{x}_1 + \delta\mathbf{x})| = \delta\mathbf{x}B'(\mathbf{x}_1)B'(\mathbf{x}_2)\dots B'(\mathbf{x}_N)$$

We assume that the difference between the variables  $\mathbf{x}$  and  $\mathbf{x} + \delta\mathbf{x}$  grows exponentially with  $N$ :

$$|B^N(\mathbf{x}_1) - B^N(\mathbf{x}_1 + \delta\mathbf{x})| = \delta\mathbf{x}e^{\lambda N}$$

$\lambda$  is called the Lyapunov exponent. We have that

$$e^{\lambda N} = B'(\mathbf{x}_1)B'(\mathbf{x}_2)\dots B'(\mathbf{x}_N) \Rightarrow \lambda = \frac{1}{N} \sum_n \ln |B'(\mathbf{x}_n)|$$

We expect  $\lambda > 0$  for a chaotic system.

## 1.2 2D billiards

In dynamical billiards, the speed is conserved, so we just consider the direction  $\phi$  in which the ball is going. We also parameterise the boundary  $C$  by  $\theta$ . This completely describes the system, so the phase space  $M$  of a dynamical billiards is two dimensional. Each point  $(\phi, \theta)$  in this space corresponds to a position on the boundary and a direction of motion. We can then build the billiard map  $B : M \rightarrow M$ :

$$(\phi_{n+1}, \theta_{n+1}) = B(\phi_n, \theta_n)$$

and obtain a sequence of points on the boundary where the ball was reflected. This describes the evolution of the system.

Say we have defined the boundary  $C$ . The normal  $\mathbf{n}$  and tangent  $\mathbf{t}$  to the boundary are

$$\mathbf{n} = \pm \frac{dC}{dr} = \pm \begin{pmatrix} \frac{\partial C}{\partial x} \\ \frac{\partial C}{\partial y} \end{pmatrix} \quad \text{and} \quad \mathbf{t} = \pm \begin{pmatrix} -\frac{\partial C}{\partial y} \\ \frac{\partial C}{\partial x} \end{pmatrix}$$

The position of the ball is defined as  $\mathbf{r} = \begin{pmatrix} x \\ y \end{pmatrix}$  and its instantaneous velocity is  $\mathbf{v} = \begin{pmatrix} \cos \phi \\ \sin \phi \end{pmatrix}$ . The angle  $\phi$  gives the direction of the ball with respect to the horizontal axis. The ball is on the boundary when  $C(\mathbf{r}) = 0$ . Given a point  $\mathbf{r}$  on the boundary and a direction  $\mathbf{v}$ , we solve

$$C(\mathbf{r} + \mathbf{v}t) = 0 \tag{1}$$

for  $t$ . This gives the distance to the next point on the boundary. The new position is then  $\mathbf{r}' = \mathbf{r} + \mathbf{v}t$ . We also need to find the new direction  $\mathbf{v}'$  after specular reflection. In the case of elastic collision, only the component of the velocity parallel to the normal of the surface is reversed:

$$\mathbf{v}' = -(\mathbf{v} \cdot \hat{\mathbf{n}})\hat{\mathbf{n}} + (\mathbf{v} \cdot \hat{\mathbf{t}})\hat{\mathbf{t}}$$

The specific methods for finding  $t$  are different for different boundaries.

### The square

We start with the unit square. The boundary  $C$  is made up of 4 line segments each parameterized by  $\lambda$ , where  $\lambda \in [0, 1]$ :

$$(x, y) = (0, \lambda), (\lambda, 0), (1, \lambda), (\lambda, 1)$$

Now if we extend these segments,  $\lambda \in \mathbb{R}$ , the ball will intersect all of them once. Our approach is to solve Equation 1 for each line segment, then check which new position  $\mathbf{r}'$  is inside the square. There are 4 equations

$$\begin{aligned} x + tv_1 &= 0, & y + tv_2 &= 0, \\ x + tv_1 &= 1, & y + tv_2 &= 1 \end{aligned}$$

and 4 solutions

$$t_0 = -\frac{x}{v_1}, \quad t_1 = -\frac{y}{v_2}, \quad t_2 = \frac{1-x}{v_1}, \quad t_3 = \frac{1-y}{v_2}$$

### The circle

The equation for the boundary of a unit circle is

$$C(\mathbf{r}) = x^2 + y^2 - 1 = 0$$

The position on the boundary is given by angle  $\theta$  and the velocity is given as before by  $\phi$ :

$$\mathbf{r} = \begin{pmatrix} x \\ y \end{pmatrix} = \begin{pmatrix} \cos \theta \\ \sin \theta \end{pmatrix} \quad \text{and } \mathbf{v} = \begin{pmatrix} \cos \phi \\ \sin \phi \end{pmatrix}$$

Then Equation 1 gives

$$(\cos \theta + t \cos \phi)^2 + (\sin \theta + t \sin \phi)^2 - 1 = 0 \quad \Rightarrow t = -2(\cos \phi + \sin \phi)$$

### The ellipse

The equation for the boundary of an ellipse with semi major axis  $a$  and semi minor axis  $b$  is

$$C(\mathbf{r}) = \frac{x^2}{a^2} + \frac{y^2}{b^2} - 1 = 0$$

with the same parametrisation as the circle,

$$\mathbf{r} = \begin{pmatrix} x \\ y \end{pmatrix} = \begin{pmatrix} \cos \theta \\ \sin \theta \end{pmatrix} \quad \text{and } \mathbf{v} = \begin{pmatrix} v_1 \\ v_2 \end{pmatrix} = \begin{pmatrix} \cos \phi \\ \sin \phi \end{pmatrix}$$

Equation 1 gives

$$\left( \frac{x + tv_1}{a} \right)^2 + \left( \frac{y + tv_2}{b} \right)^2 = 0 \quad \Rightarrow \epsilon + t^2 \left( \frac{v_1^2}{a^2} + \frac{v_2^2}{b^2} \right) + t \left( \frac{2xv_1}{a^2} + \frac{2yv_2}{b^2} \right) = 0$$

where  $\epsilon = \frac{x^2}{a^2} + \frac{y^2}{b^2} - 1$ . We are solving for the boundary so  $\epsilon = 0$ .

Then the solution  $t \neq 0$  is

$$t = -2 \left( \frac{1}{\frac{v_1^2}{a^2} + \frac{v_2^2}{b^2}} \right) \left( \frac{v_1 x}{a^2} + \frac{v_2 y}{b^2} \right)$$

## 2 Integrable billiards

### 2.1 The square

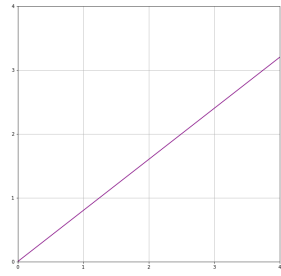


Figure 1: The grid

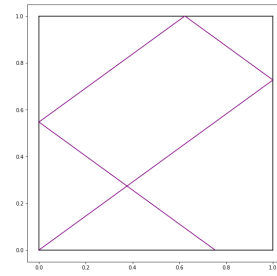


Figure 2: Reflections

The square is usually solved by unfolding the grid, see Figure 1. The trajectories in Figure 2 are the reflections of the trajectory in each square in the grid. In this example we simply fold vertically then horizontally then repeat.

We find periodic trajectories as expected, and some pretty patterns, Figures 3, 4, 5.

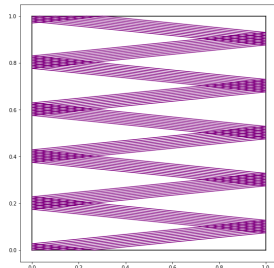


Figure 3:  $\phi = 0.1$

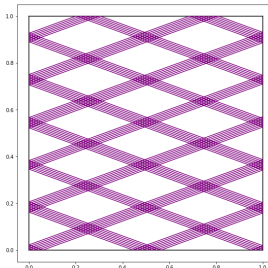


Figure 4:  $\phi = \pi/9$

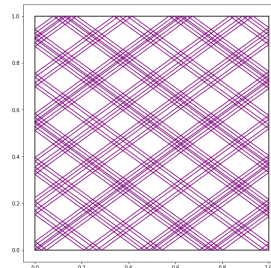


Figure 5:  $\phi = \pi/5$

If the initial velocity  $\phi$  is an irrational multiple of  $\pi$ , the trajectory is not periodic (Figure 6), and will completely fill up the square (Figure 7). We say that the trajectory is dense in the square.

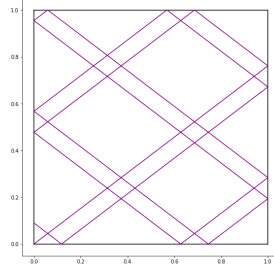


Figure 6: 15 trajectories for  $\phi = \pi(\frac{1}{\sqrt{2}} - \frac{1}{2})$

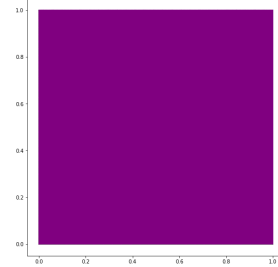


Figure 7: 2000 trajectories for  $\phi = \pi(\frac{1}{\sqrt{2}} - \frac{1}{2})$

This system is stable: for a very large number of trajectories, the periodic behavior stays the same. When we add an offset  $\delta$  in the initial velocity  $\phi$ , the periodic motion is just shifted, Figures 8- 10

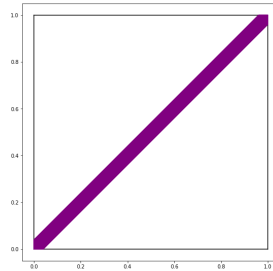


Figure 8:  $\delta = 10^{-4}$

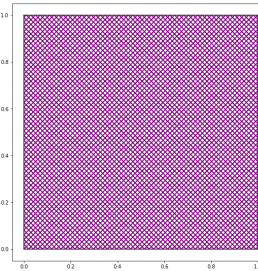


Figure 9:  $\delta = 10^{-2}$

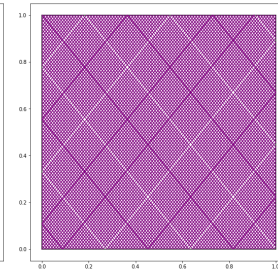


Figure 10:  $\delta = 10^{-1}$

## 2.2 The circle

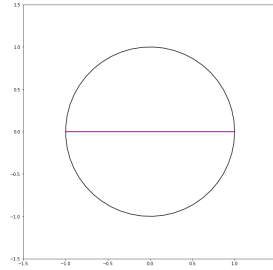


Figure 11: The 2-cycle

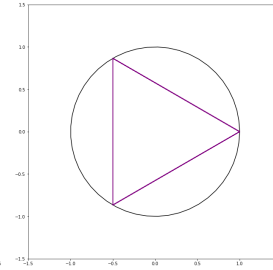


Figure 12: The 3-cycle

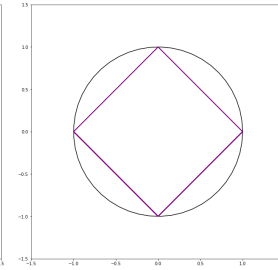


Figure 13: The 4-cycle

The trajectories in the circle are completely determined by  $\theta$  due to the rotational symmetry.

The billiard map is 1-dimensional:

$$\theta_{n+1} = \theta_n + \alpha$$

Some trajectories, which we call cycles, are periodic. An N-cycle is a trajectory that repeats after N reflections off the boundary. These trajectories are straightforward to solve analytically. The  $n = 0, 1, 2, \dots, N$  angles are given by the map

$$\theta_n = \theta_0 + \frac{2\pi n}{N}$$

The analytic variable  $\alpha = 2\pi n/N$  and the usual velocity angle  $\phi$  are linked by

$$\pi = \alpha + 2\theta = \phi + \theta \Rightarrow \phi = \frac{\alpha - \pi}{2}$$

The 3-cycle is a triangle inside the circle:  $\alpha = \frac{2\pi n}{3}$ . Taking  $\varphi_0 = 0$ , we have

$$\varphi_1 = \frac{2\pi}{3}, \varphi_2 = \frac{4\pi}{3} \text{ and } \varphi_3 = 2\pi = \varphi_0$$

Indeed this is what we find in the simulation, taking  $\theta = 0$  and  $\phi = \frac{5\pi}{6}$  (Figure 12).

The 4-cycle is a square inside the circle:  $\alpha = \frac{2\pi n}{4}$ . Taking  $\varphi_0 = 0$  again, we have

$$\varphi_1 = \frac{\pi}{2}, \varphi_2 = \pi \text{ and } \varphi_3 = \frac{3\pi}{2}$$

In the simulation we take  $\theta = 0$  and  $\phi = \frac{3\pi}{4}$  and find the expected results (Figure 13).

There are two 5-cycles: one where the trajectory forms a pentagon with  $\alpha = \frac{2\pi n}{5}$ , and one where the trajectory goes around the circle twice before repeating, creating a pentagram:  $\alpha = \frac{4\pi n}{5}$ .

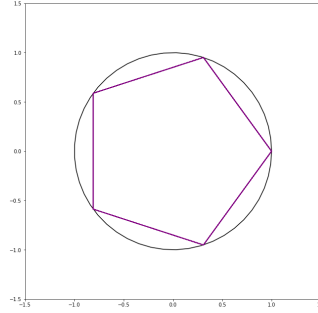


Figure 14: Pentagon

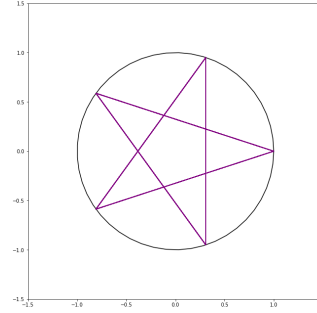


Figure 15: Pentagram

The pentagon 5-cycle has points of intersection at

$$\varphi_0 = 0, \varphi_1 = \frac{2\pi}{5}, \varphi_2 = \frac{4\pi}{5}, \varphi_3 = \frac{6\pi}{5} \varphi_4 = \frac{8\pi}{5}$$

and  $\phi = \frac{7\pi}{10}$  in the simulation.

The pentagram 5-cycle is such that

$$\begin{aligned} \varphi'_0 &= 0, & \varphi'_1 &= \frac{4\pi}{5} = \varphi_2, & \varphi'_2 &= \frac{8\pi}{5} = \varphi_4, & \varphi'_3 &= \frac{12\pi}{5} = \frac{2\pi}{5} = \varphi_1, \\ \varphi'_4 &= \frac{16\pi}{5} = \frac{6\pi}{5} = \varphi_3 & \text{and } \phi' &= \frac{9\pi}{10} \end{aligned}$$

We can keep decreasing  $\alpha$  and obtain higher cycles. As  $N$  increases, so does the number of distinct  $N$ -cycles. This is because of the periodicity: more reflections give more ways to fit the cycle inside the circle.

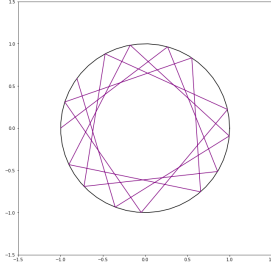


Figure 16: Non periodic motion

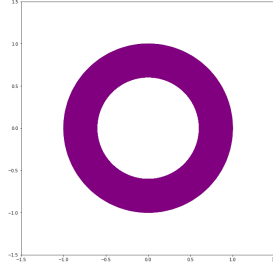


Figure 17: Dense trajectory

When  $\alpha$  is an irrational multiple of  $\pi$ , the trajectory will never repeat. But unlike the square, the trajectories inside a circle are not dense. Taking for example  $\alpha = \sqrt{2}\pi$ , so  $\phi = \pi(\frac{1}{\sqrt{2}} - \frac{1}{2})$ , we can see from the 15 trajectories plot that it doesn't repeat. For 1000 trajectories, they fill up the annulus (Figure 16 and 17).

There is always an inner circle that is empty of any trajectories. Obviously crossing the center gives a 2-cycle, and for any initial direction above (or below) the center, the trajectories will fill an annulus. The further away from the center, the thinner the annulus. Figures 18 to 21 show 100 trajectories for initial directions ranging from close to 0, to close to  $\pi/2$ .

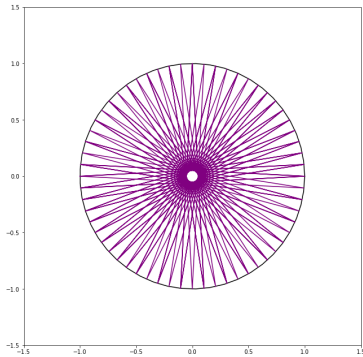


Figure 18:  $\theta = \pi$  and  $\phi = \pi/60$

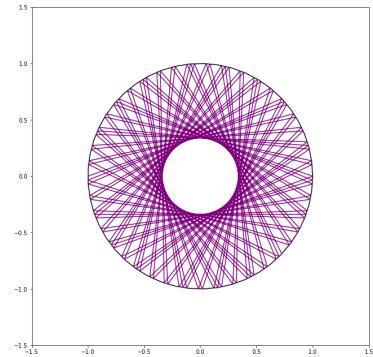


Figure 19:  $\theta = \pi$  and  $\phi = \pi/9.1$

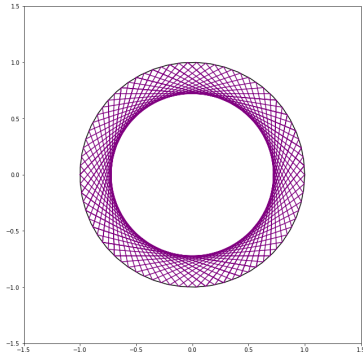


Figure 20:  $\theta = \pi$  and  $\phi = \pi/3.9$

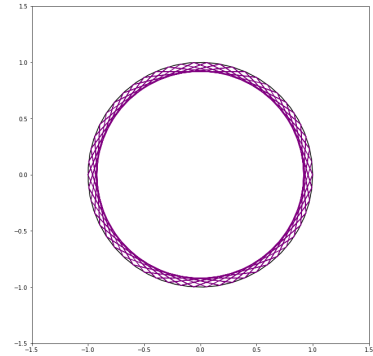


Figure 21:  $\theta = \pi$  and  $\phi = \pi/2.7$

Like the square, the circle has enough symmetry to be stable. Figures 22-24 show the different shifted periodic motions for different  $\delta$ .

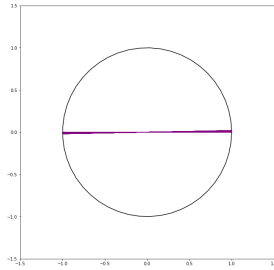


Figure 22:  $\theta = \pi$  and  $\phi = 10^{-4}$

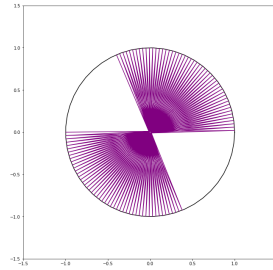


Figure 23:  $\theta = \pi$  and  $\phi = 10^{-2}$

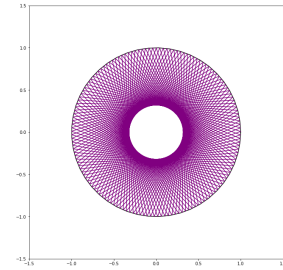


Figure 24:  $\theta = \pi/2$  and  $\phi = \pi/3.5 + 1$

## 2.3 The ellipse

Recall that Equation 1 gave a quadratic equation:

$$\epsilon + t^2 \left( \frac{v_1^2}{a^2} + \frac{v_2^2}{b^2} \right) + t \left( \frac{2xv_1}{a^2} + \frac{2yv_2}{b^2} \right) = 0$$

which we solved for  $t$  assuming that the boundary  $\epsilon = \frac{x^2}{a^2} + \frac{y^2}{b^2} - 1 = 0$ .

However  $\epsilon$  is not always exactly 0 (this is the case when  $a$  or  $b$  are not integers), and this leads to significant numerical errors. In Figure 25, we have 50 trajectories for  $\theta = \pi$  and  $\phi = 0$ . We expect the trajectories to stay on the line crossing the two foci, but the accumulation of errors quickly makes the lines diverge.

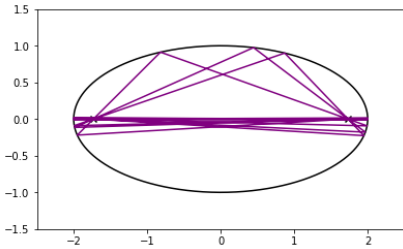


Figure 25: Errors in 50 trajectories of  $\theta = \pi$  and  $\phi = 0$

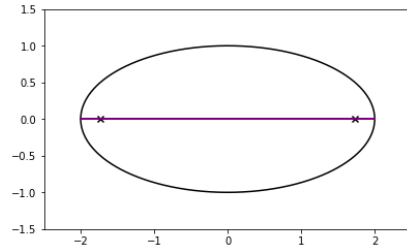


Figure 26: Expected results in 50 trajectories of  $\theta = \pi$  and  $\phi = 0$

To resolve this we set the position  $(x', y') = (x + tv_1, y + tv_2)$  to position  $(X', Y')$  on the boundary, by solving  $\epsilon = 0$ :

$$X' = \text{sign}(x') a \sqrt{1 - \frac{y'^2}{b^2}}$$

$$Y' = \text{sign}(y') b \sqrt{1 - \frac{x'^2}{a^2}}$$

This gives the expected results in the simulation, Figure 26 with the same initial conditions.

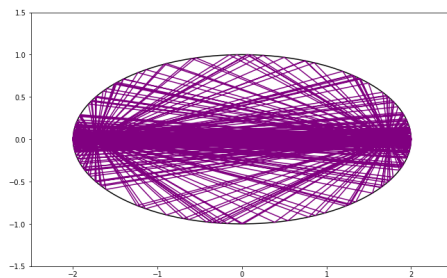


Figure 27: Divergence in  $\theta = \pi$  and  $\phi = \delta = 10^{-8}$

As a sanity check, we can set  $a, b = 1$  so that the ellipse becomes a circle. The simulation runs as expected, giving the same plots as in the previous section.

The  $\theta = \pi, \phi = 0$  trajectories are very sensitive to an offset (in  $\theta$  or in  $\phi$ , they give basically the same results). The trajectory diverges completely for  $\delta = 10^{-8}$  (Figure 27), whereas in the circle it only started to diverge slightly at  $\delta = 10^{-4}$ . This is because of the shape of the ellipse: the error will keep growing with each trajectory. The first intercept is slightly away from point 0, then the bounce back is even further away from  $\pi$ , etc... For the circle, the offset stays constant: the trajectories are just shifted.

Interestingly, we find some periodic behavior again as  $\delta$  increases (Figures 28–31). Notably Figure 10 with  $\delta = 10^{-2}$  has unexpected behaviour.

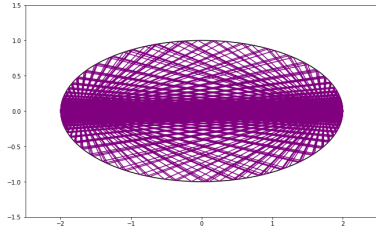


Figure 28:  $\delta = 10^{-6}$

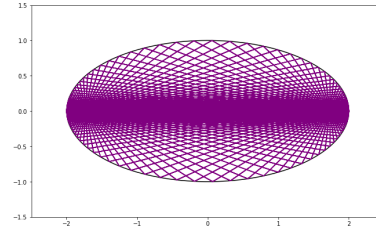


Figure 29:  $\delta = 10^{-4}$

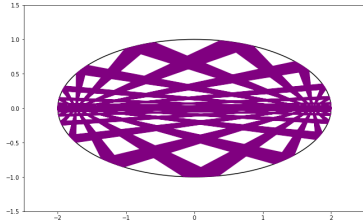


Figure 30:  $\delta = 10^{-3}$

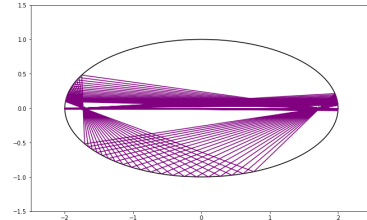


Figure 31:  $\delta = 10^{-2}$

We observe two general types of behavior, depending on the initial trajectory with respect to the foci. When the initial trajectory is in between the foci, all following reflections will also stay inside, Figure 32.

Similarly if the initial trajectory is outside the foci, then all other reflections also stay outside, Figure 33.

There is a special case when the initial trajectory crosses a focus point: it converges to the line crossing both foci. With  $a = 2$ , the distance to each foci is  $\sqrt{3}$ . The ellipse is centered at 0 so taking  $(x, y) = (\sqrt{3}, 0.5)$  and  $\theta = \pi/2$ , we indeed find the expected results, Figure 34.

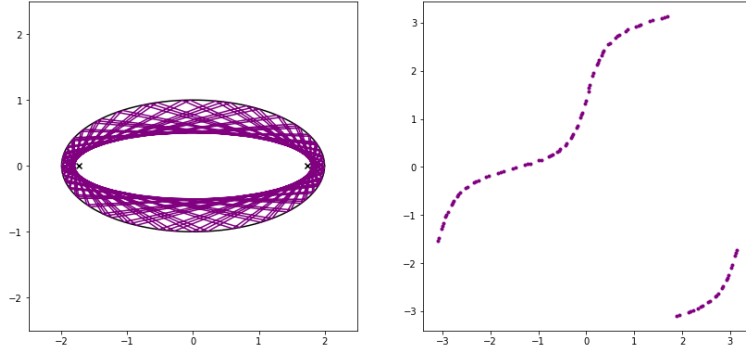


Figure 32: 100 trajectories for  $\theta = \pi$  and  $\phi = 5\pi/6$  and the phase map

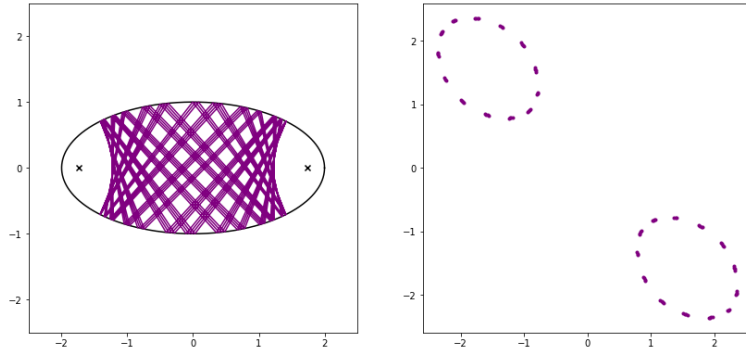


Figure 33: 100 trajectories for  $\theta = 2\pi/3$  and  $\phi = 7\pi/4$  and the phase map

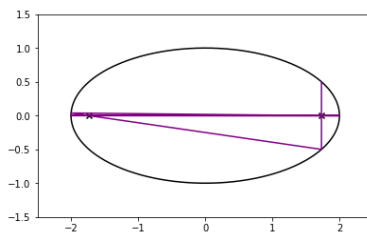


Figure 34: 10 trajectories for  $\theta = \pi/2$  and  $\phi = \text{arctan2}(y/b, x/a)$

We can also plot the phase map of  $\phi$  (current  $\phi$  against previous) for different initial conditions to have an idea of the global behavior. Figure 35 shows the phase map of 20 different initial conditions.

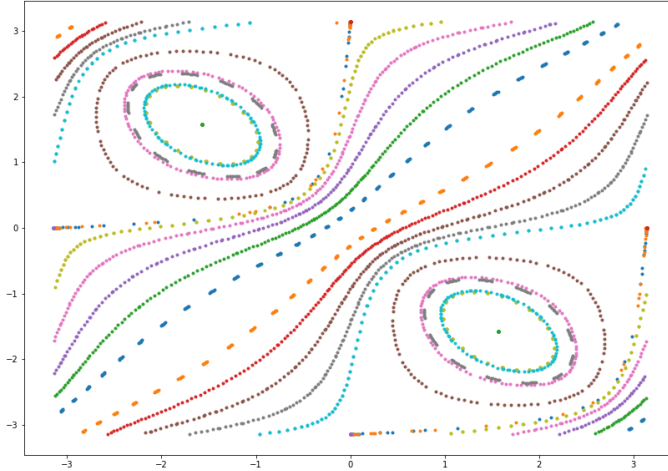


Figure 35: Phase portrait of the ellipse for 20 different initial conditions, 200 trajectories each

### 3 Chaotic billiards

#### 3.1 The Bunimovich stadium

##### Implementation

The Bunimovich stadium is made up of two half-circles and two straight line segments. The radius of the semi-circles is  $r$  and  $L$  is the length of half a line segment (Figure 36).

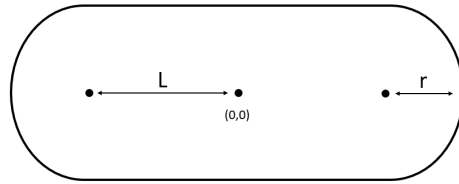


Figure 36: Stadium with  $r = 1$  and  $L = 2$

We use a similar approach as the square: given an initial position and a velocity, we find the intersection of that trajectory with every boundary, including the two whole circles. There will be two intersections per circle, and one per line, so 6 distances total. The trajectory may not always actually cross the circle, so some values of  $t$  will be complex, which we ignore. One of them will be (close to) zero- the current position. From the rest of  $t$  values, only one is a valid

position on the stadium. It is found by updating the position and checking if both its x and y components are on the stadium.

Let  $T$  be the boundary for the top line,  $B$  for the bottom line,  $L$  for the left semi-circle and  $R$  for the right semi-circle. Equation 1 gives:

$$\begin{aligned} T : y + t_T v_2 &= r, \quad B : y + t_B v_2 = -r, \\ L : (x + t_L v_1 + L)^2 + (y + t_L v_2)^2 - r^2 &= 0, \\ R : (x + t_R v_1 - L)^2 + (y + t_R v_2)^2 - r^2 &= 0 \end{aligned}$$

The solution to the top and bottom line is simply

$$t_T = \frac{r - y}{v_1}, \quad t_B = \frac{-r - y}{v_1}$$

The circles are quadratic in  $t$ :

$$t_{L,R} = t_{L,R}^2 + t_{L,R}(2v_1(x \pm L) + 2yb_2) + (x \pm L)^2 + y^2 - r^2 = 0$$

Like before,  $(x \pm L)^2 + y^2 - r^2 = 0$ , but only for one of the circles at a time, so we solve the full equations.

## Results

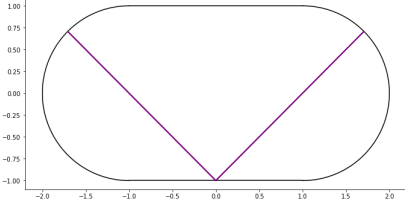


Figure 37: A 4-cycle

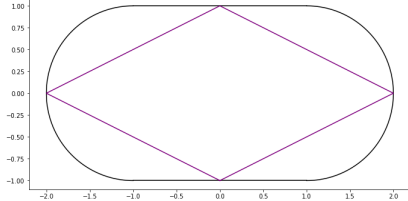


Figure 38: Another 4-cycle

We find some periodic trajectories around the stadium (37, 38), but they are unstable: Figure 39 shows 20 trajectories for initial position  $(-2, 0)$  and initial velocity  $\phi = \pi/3$ . Figure 40 is the same initial conditions but with 50 trajectories.

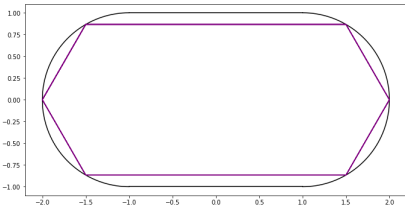


Figure 39: 20 trajectories

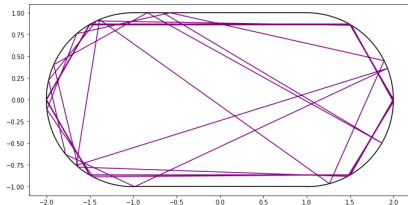


Figure 40: 50 trajectories

We know that this instability is not due to numerical errors because the 2-cycles are stable: see Figure 41 and Figure 42.

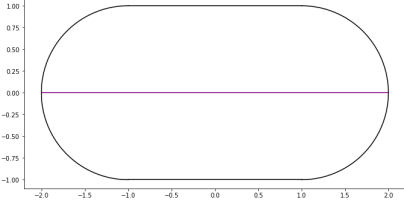


Figure 41: 500 trajectories of a 2-cycle

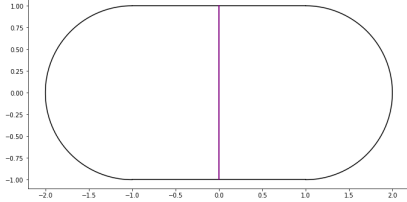


Figure 42: 500 trajectories of another 2-cycle

Like the ellipse, the stadium is not symmetric enough to preserve periodic motions: Figure 43 shows 20 trajectories of  $\phi = \pi/3 + \delta$ , with offset  $\delta = 10^{-5}$ . Figure 44 shows 100 trajectories of  $\phi = \delta = 10^{-7}$ . The error from the offset increases just like the ellipse, but this time because of the length of the stadium: the little deviation grows over the distance travelled by the ball.

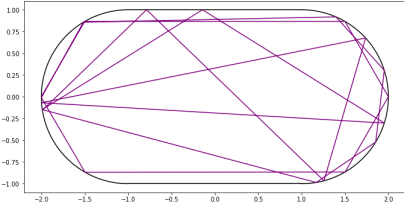


Figure 43: Offset  $\delta = 10^5$  in initial velocity  $\phi = \pi/3 + 10^{-5}$

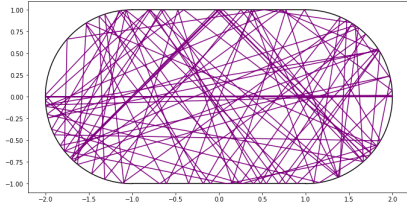


Figure 44: 100 trajectories of  $\phi = \delta = 10^{-7}$

We can already see that the trajectories are chaotic. Another hint is from the phase space. Figure 45 shows the position angles  $\theta$  against the velocity angles  $\phi$  for 100000 trajectories.

It is not ideal to use the variable  $\theta$ . This is because, for a given increment in the angle, the arc length covered is different at different points in the stadium. This means  $\theta$  is not uniform, and can hide some information about the system. We can still observe ergodicity in the phase space, as it gets filled up in the allowed regions. The ball has taken close to all the trajectories available.

### The Lyapunov exponent

In a billiard, the degrees of freedom are all bounded:  $\phi$  and  $\theta$  are periodic, and the length of a trajectory has maximum  $2r + 2L$ . When a billiard is chaotic, the separation between infinitesimally close trajectories will grow exponentially at first but then plateaus because of the periodicity.

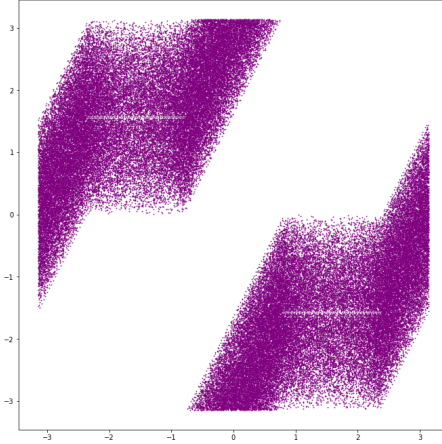


Figure 45: Phase space for  $\phi = \pi/3$

Figure 46 and 47 show the velocity and distance of two trajectories with the same initial condition but an offset of  $10^{-12}$  in  $\theta$  and  $\phi$ . To characterise the growth in separation between trajectories, we calculate an approximate Lyapunov exponent.

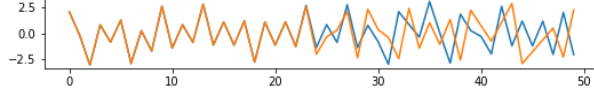


Figure 46: The velocity  $\phi$  over trajectories

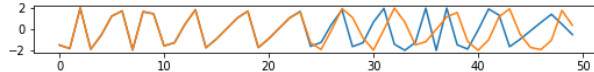


Figure 47: The distance over trajectories

We use

$$|B^N(\mathbf{x}_1) - B^N(v_1 + \delta\mathbf{x})| = \delta\mathbf{x}e^{\lambda N}$$

to find the Lyapunov  $\lambda$ . Here  $\mathbf{x} = (\theta, \phi)$  and  $\mathbf{x} + \delta\mathbf{x} = (\theta + \delta, \phi + \delta) \equiv (\theta_\delta, \phi_\delta)$ , with  $\delta = 10^{-12}$ . We plot

$$\ln(\sqrt{(\theta_N - \theta_{\delta N})^2 + (\phi_N - \phi_{\delta N})^2})$$

against  $N$ , the number of trajectories. The gradient of this curve (the exponent) is the Lyapunov in phase space  $\lambda_P$ .

We can also compute the Lyapunov in Euclidean space  $\lambda_E$  in a similar way, with

$$\ln(\sqrt{(x_N - x_{\delta N})^2 + (y_N - y_{\delta N})^2})$$

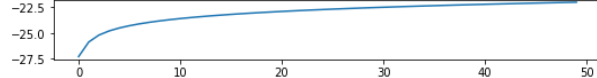


Figure 48: The Lyapunov over 50 trajectories,  $L = 0$

As expected, for a circle,  $L = 0$ , the curve stays approximately around  $\ln(\delta)$  (Figure 48).

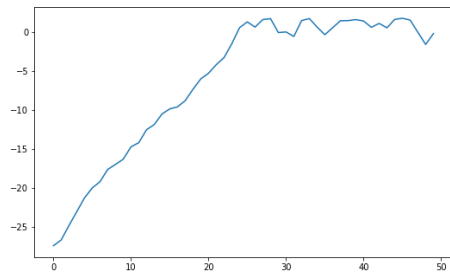


Figure 49: The Lyapunov over 50 trajectories,  $L = 1$

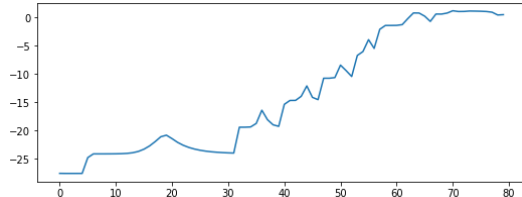


Figure 50: The Lyapunov over 80 trajectories,  $L = 10$

Figures 49 and 50 show the Lyapunov for  $L = 1$ , 50 trajectories and  $L = 10$ , 80 trajectories. The second stadium reaches the plateau after more trajectories since it takes more steps to be periodic. It also grows slower because the shape is dominated by the straight lines, which don't generate chaotic behavior.

We need to manually choose the trajectories that will contribute to the Lyapunov. For  $L = 0$ , we can see from Figure 48 that we need to cut off the first  $\sim 5$  trajectories, and go up to  $\sim 40$ . This gives  $\lambda_P \approx 0.053$  and  $\lambda_E \approx 0.039$ . This was to be expected (for non periodic motion): for a circle, it so happens that the Lyapunov is positive, but close to 0.

For  $L = 1$ , the exponential growth is from 0 to  $\sim 25$  trajectories. These give  $\lambda_P \approx 1.076$  and  $\lambda_E \approx 1.081$ . These values confirm that the stadium is a chaotic system.

For  $L = 10$ , we calculate the Lyapunov from 30 to 65 trajectories:  $\lambda_P \approx 0.712$  and  $\lambda_E \approx 0.427$ .

We continue like this and plot the phase space Lyapunov against the length of the stadium, Figure 51.

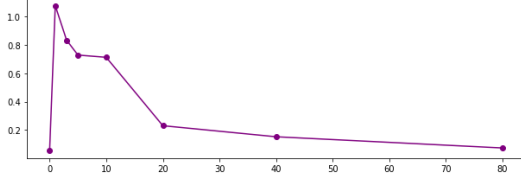


Figure 51: The Lyapunov against the length of the stadium

We can see that the Lyapunov peaks at  $L = 1$  then decreases to 0 exponentially.

There is a better, proper way to calculate the Lyapunov that would provide much more accurate results and automate this process. This is beyond our reach for now.

### 3.2 The half stadium

So far every system we have considered preserved direction: the ball never goes clockwise if it started counterclockwise, vice versa. In the half stadium however, the direction can be reversed, Figure 52. This is more clear in Figure 53, where we start in the top right corner and go in the direction of  $\phi = -\pi/2 + 10^{-4}$ . The trajectory starts clockwise and ends up counterclockwise.

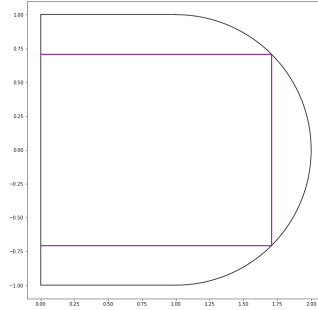


Figure 52: The reversed mode

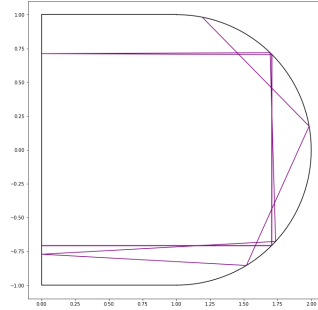


Figure 53: A reversed trajectory

The semi-circle,  $L = 0$ , turns out to be integrable. Its behavior is very similar to that of the circle. The first few trajectories don't seem regular, Figure 54, but they quickly fall into a pattern, Figures 55 and 56. We can almost get the trajectories to be dense, Figure 57 with  $\phi = \pi/2.01$ . There are also some strange periods, Figure 58. Figure 59 shows the phase portrait. The vertical lines are from the straight line in the half stadium and the diagonal lines are from the circular part.

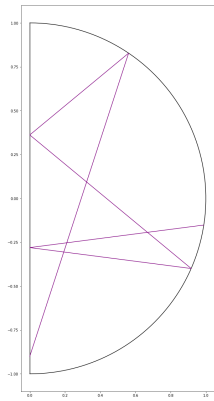


Figure 54

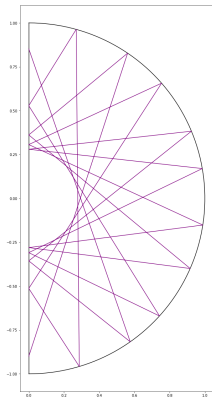


Figure 55

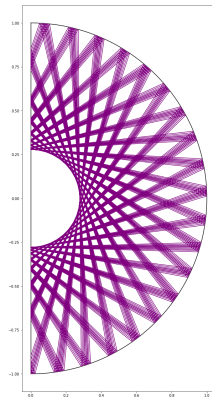


Figure 56

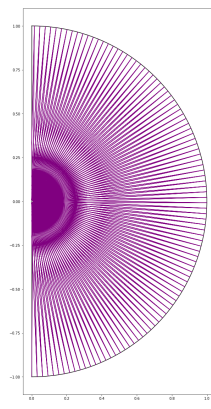


Figure 57: A non-periodic trajectory

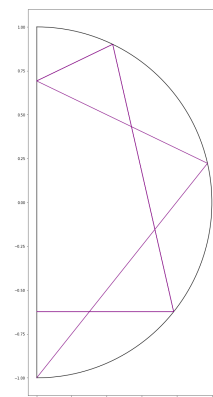


Figure 58: A periodic trajectory

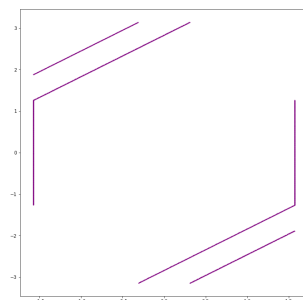


Figure 59: The phase space of the semi circle

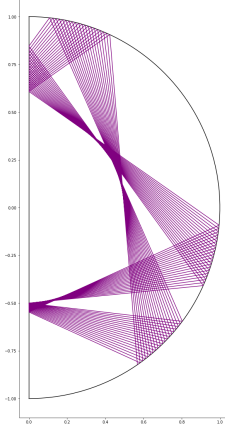


Figure 60: A  
strange pattern

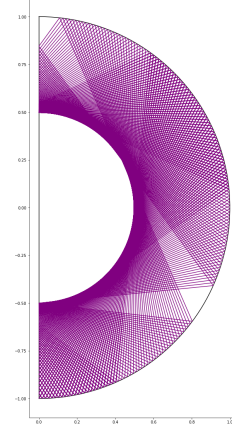


Figure 61: More  
trajectories

When  $L > 0$ , the half stadium is chaotic, like the Bunimovich. The phase space when the initial position is on the line is similar to the Bunimovich, but  $\theta$  ranges from  $\pi/2$  to  $-\pi/2$  (Figure 62). It also has extra vertical lines on the edge.

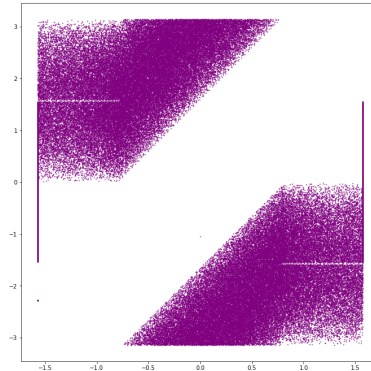


Figure 62: The phase space of the half stadium,  $L = 1$

There is another mode that can reverse the trajectory, Figure 63. This mode is unstable, Figure 64. Its phase space is strange: Figure 65 shows 100000 trajectories, and Figure 66 shows 200000 trajectories. It's not clear if the filling of the space is due to the reverse in direction.

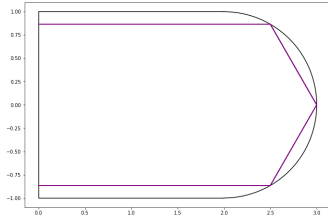


Figure 63: A reversed trajectory

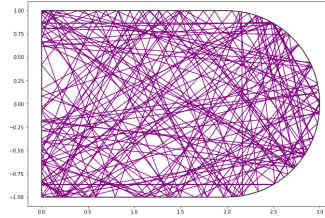


Figure 64: Unstable

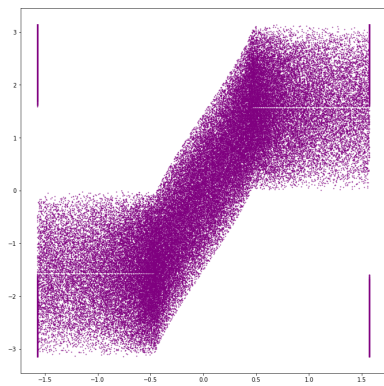


Figure 65: 100000 trajectories

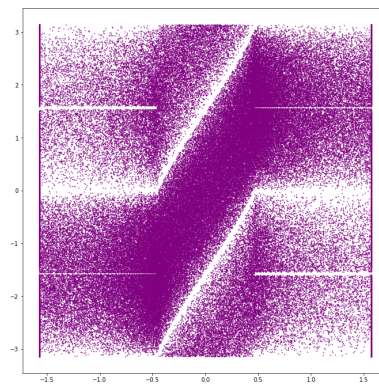


Figure 66: 200000 trajectories

We also calculate the Lyapunovs using the same method as before. For  $L = 0$ , the Lyapunov is close to 0 as expected:  $\lambda_P \approx 0.065$ . For  $L = 1$ , we can see From Figure 67 that we need to calculate  $\lambda$  from 0 to  $\sim 35$  trajectories. This gives  $\lambda \approx 0.732$ .

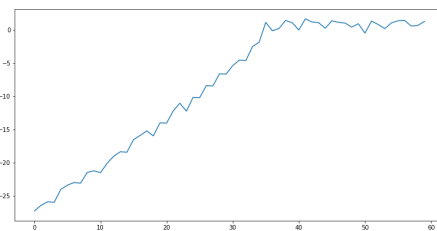


Figure 67: The Lyapunov over 60 trajectories,  $L = 1$

We continue like this and get Figure 68. The Lyapunov peaks at  $\lambda_P \approx 0.8$  when  $L = 3$ . We conclude that the Bunimovich stadium is more chaotic than the half stadium.

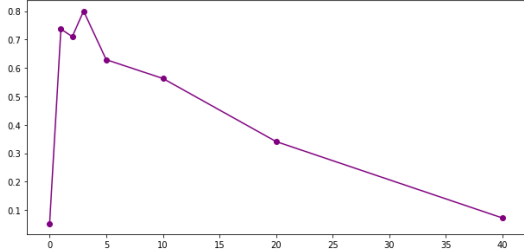


Figure 68: The Lyapunov against the length of the half stadium

## Further work

Further investigations should be carried out to understand the nature of the phase space in Figure 66.  
The transition from regular to chaotic behaviour as  $L$  increases from 0 could be interesting for both stadiums. This would require a more efficient code for calculating the Lyapunov.

## References

- [1] S. Tabachnikov, *Geometry and billiards*, (2005) <https://api.semanticscholar.org/CorpusID:117337589>.
- [2] M. Turaev, *Numerical experiments in billiards*, (2016) <https://urn.kb.se/resolve?urn=urn:nbn:se:uu:diva-279462>.
- [3] S. W. Park, *An introduction to dynamical billiards*, (2014) <https://api.semanticscholar.org/CorpusID:17759434>.
- [4] L. A. Bunimovich, “On the ergodic properties of certain billiards”, *Functional Analysis and Its Applications* **8**, 254–255 (1974).